

Metabolite changes in HT-29 xenograft tumors following HIF-1 α inhibition with PX-478 as studied by MR spectroscopy *in vivo* and *ex vivo*

Bénédicte F. Jordan,^{1,2} Kvar Black,¹ Ian F. Robey,¹ Matthew Runquist,³ Garth Powis⁴ and Robert J. Gillies^{1*}

¹Department of Biochemistry and Molecular Biophysics, Arizona Cancer Center, Tucson, AZ 85724, USA

²Laboratory of Biomedical Magnetic Resonance, Université Catholique de Louvain, B-1200 Brussels, Belgium

³Division of Biotechnology, Arizona Research Laboratories, Tucson, AZ 85721, USA

⁴Department of Pathology, Arizona Cancer Center, University of Arizona, Tucson, AZ 85724, USA

Received 20 May 2005; Revised 11 July 2005; Accepted 12 July 2005

ABSTRACT: The hypoxia-inducible transcription factor (HIF-1 α) plays a central role in tumor development. PX-478 is an experimental anti-cancer drug known to inhibit HIF-1 α in experimental tumors. The purpose of this study was to identify MRS-visible metabolic biomarkers for PX-478 response prior to phase I/II clinical trials. Single-voxel *in vivo* localized ¹H spectra were obtained from HT-29 tumor xenografts prior and up to 24 h after treatment with a single dose of PX-478. Profiles of water-soluble and lipophilic metabolites were also examined *ex vivo* with both ¹H and ³¹P spectroscopy for peak identification and to interrogate the underlying biochemistry of the response. The total choline (tCho) resonance was significantly decreased *in vivo* 12 and 24 h following treatment with PX-478 and this was confirmed with high-resolution ¹H and ³¹P MRS. In non-aqueous extracts, significant reductions in cardiolipin, PtdEtn (phosphatidylethanolamine) and PtdI (phosphatidylinositol) were seen in response to PX-478. Although there were trends to a decrease in lactate (and lipid) resonances *in vivo* and *ex vivo*, these changes were not significant. This is in contrast to inhibition of *in vitro* glucose consumption and lactate production by PX-478 in HT-29 cells. The significant and robust change in tCho has identified this as a potential ¹H MRS-visible biomarker for drug response *in vivo* while high-resolution spectroscopy indicated that GPC, PC, myoI, PE, GPE, CL, PtdEtn and PtdI are potential *ex vivo* response biomarkers. Copyright © 2005 John Wiley & Sons, Ltd.

KEYWORDS: HT-29 tumor xenografts; HIF-1 α ; PX-478; Cancer chemotherapy; H-MRS

INTRODUCTION

Solid tumors with areas of hypoxia are the most aggressive and difficult to treat.¹ Even micrometastases have areas of hypoxia at the growing edge where tumor growth outstrips new blood vessel formation.² Hypoxic cancer cells can survive the hostile microenvironment by changing to a glycolytic metabolism,^{3,4} becoming resistant to programmed cell death (apoptosis),⁵ and producing factors such as vascular endothelial growth factor (VEGF)

that stimulate new blood vessel formation from existing vasculature (angiogenesis) leading to increased tumor oxygenation and growth.⁶ The cellular response to hypoxia is often mediated through the hypoxia inducible factor-1 (HIF-1) transcription factor.^{7,8} HIF-1 is heterodimer consisting of HIF1- α and HIF-1 β subunits which associate in the cytosol prior to transport to the nucleus⁹ where they bind to hypoxia response element (HRE) DNA sequences.¹⁰ HIF-1 β is constitutively expressed and its levels are not changed by hypoxia.¹¹ HIF-1 α is constitutively expressed but, under aerobic conditions, it is rapidly degraded in normal cells by the ubiquitin-26S proteasome pathway such that it is virtually undetectable.¹² Under conditions of hypoxia, HIF-1 α degradation is inhibited and HIF-1 α protein levels increase, resulting in an increase in HIF-1 transactivating activity.

HIF-1 α expression has been detected in the majority of solid tumors examined including brain, bladder, breast, colon, ovarian, pancreatic, renal and prostate, whereas no expression was detected in surrounding normal tissue, nor was it detected in benign tumors.¹³ Clinically, HIF-1 α over-expression has been shown to be a marker of

*Correspondence to: R. J. Gillies, Department of Biochemistry and Molecular Biophysics, Arizona Cancer Center, Tucson, AZ 85724, USA.

E-mail: gillies@u.arizona.edu

Contract/grant sponsor: PHS; contract/grant numbers: U54 CA90821; CA077575; R24 CA083148; P30 CAQ3074; CA98920.

Abbreviations used: HIF, hypoxia-inducible transcription factor; tCho, total choline; tCr, total creatine; choline, Cho; PC, phosphocholine; GPC, glycerolphosphocholine; mI, myoinositol; Tau, taurine; Ala, alanine; Lac, lactate; PDE, phosphodiester; PME, phosphomonoester; PE, phosphoethanolamine; GPE, glycerophosphoethanolamine; PtdEtn, phosphatidylethanolamine; PtdCho, phosphatidylcholine; PtdI, phosphatidylinositol; SM, sphingomyelin; CL, cardiolipin.

highly aggressive disease and has been associated with poor prognosis and treatment failure in a number of cancers including breast, ovarian, cervical, oligodendroglioma, esophageal and oropharyngeal.^{14–18} HIF-1 α levels correlate with tumor grade as well as vascularity.^{11,19} These observations suggest that HIF-1 mediates hypoxia-induced VEGF expression in tumors leading to highly aggressive tumor growth.

PX-478, (*S*)-2-amino-3-[4'-*N,N*-bis(2-chloroethyl)amino]phenylpropionic acid *N*-oxide dihydrochloride, is a novel agent that suppresses both constitutive and hypoxia-induced levels of HIF-1 α in cancer cells.²⁰ The inhibition of tumor growth by PX-478 is positively associated with HIF-1 α levels in a variety of different human tumor xenografts in SCID mice. Welsh *et al.* showed a reduction in HIF-1 α levels in HT-29 tumors 2 h after a single dose of PX-478 that returned to normal 8 h after treatment. Similar changes were also observed with VEGF. More recently, we characterized the effect of PX-478 on HT-29 xenograft tumors using dynamic contrast enhanced and diffusion-weighted MRI and showed that this drug induced early changes in vascular permeability followed by large changes in cellularity.²¹ The time course of this effect was fairly different from the changes in HIF-1 α since the effects on tumor permeability and cellularity were maximum by 24 h and returned to baseline by 48 h post-treatment. This investigation is a follow-up to these studies to determine if there are metabolic changes that occur in response to PX-478 that are visible *in vivo* by MRS.

MRS provides non-invasive biochemical information on tissues and can be used to study the physiopathology of tumors and tumor cells *in vitro*, *ex vivo* and *in vivo*. It is also used to assess tumor response to therapy both in experimental and in human tumors.^{22–26} ¹H spectroscopic studies usually focus on choline-containing compounds and lactate, which have been shown to be elevated in a variety of human tumors compared with the normal tissue,^{27–30} while various phosphorus-containing components of phospholipid metabolism, such as phosphomonoesters (PMEs) and phosphodiesteres (PDEs), are readily observed using ³¹P MRS. Clinically, MRS has already demonstrated the potential for improved diagnosis, staging and treatment planning of brain, breast and prostate cancer.^{22,31–37}

The aim of this study was to identify metabolic markers for hemodynamic changes consequent to HIF-1 α inhibition and tumor response to PX-478 treatment. For that purpose, we first performed *in vivo* single voxel ¹H spectroscopy in HT-29 xenograft tumors before and until 24 h after treatment with PX-478. Second, we studied profiles of water-soluble and lipophilic spectral components with both ¹H and ³¹P *in vitro* spectroscopy on extracts from HT-29 tumors treated with 0–150 mg/kg of PX-478. Finally, in order to characterize further the metabolic changes observed *in vivo* and *ex vivo*, lactate production and glucose

uptake were measured on HT-29 cells before and after treatment with PX-478.

EXPERIMENTAL

Cell line and tumor implantation

HT-29, a tumorigenic, non-metastatic human colon carcinoma cell line, was obtained from the American Tissue Type Collection (Rockville, MD). Cells were passaged twice weekly with a 1:2 split and cultured in Dulbecco's modified Eagle's medium (DMEM:F12) supplemented with 10% fetal bovine serum (HyClone, Fort Collins, CO). For inoculation, $\sim 10^6$ cells in 0.1 ml of media were injected subcutaneously into the right flank of female severe combined immunodeficient (SCID) mice of age 5–6 weeks (obtained from the Arizona Cancer Center Experimental Mouse Shared Services). Mice developed palpable tumors within 1 week of inoculation. Tumors were allowed to grow to 100–500 mm³ prior to imaging. All animal protocols were approved by the University of Arizona Institutional Animal Care and Use Committee (IACUC).

Treatments

PX-478 was provided by Prolx Pharmaceuticals (Tucson, AZ) and was prepared fresh each day in 0.9% NaCl as a 10 mg/ml solution and administered *i.p.* to the mice within 30 min of preparation. For *in vivo* spectroscopy, mice were treated with 125 mg/kg of PX-478 ($n = 10$) and were studied 0, 1, 2, 12 and 24 h later (mice were removed from the magnet between the 2 and 12 h time points and between the 12 and 24 h time points). Mice were anesthetized using 1.0–2.0% isoflurane carried in oxygen. Body temperature was maintained at 37 °C with a circulating water blanket and was monitored using a rectal Luxtron fluoroptic thermometer (Luxtron, Santa Clara, CA). For *ex vivo* high-resolution spectroscopy, mice were treated with either vehicle ($n = 3$) or with increasing doses of PX-478 (50–200 mg/kg, $n = 8$) and killed 24 h later. Tumor was excised and immediately clamped and frozen in liquid nitrogen and stored at –80 °C.

Tumor extracts

The freeze-clamped tumors were treated as follows. Extraction of the water-soluble metabolites and of the lipids was performed by a dual phase extraction (DPE) method.³⁴ Tissue samples were placed in 10 ml of ice-cold methanol containing 0.4 mM phenylphosphonic acid (Aldrich, Milwaukee, WI) for 1 h. The tissue was then homogenized in the methanol solution within 1 min. An equal volume of chloroform was added to the homogenate and the mixture was vigorously vortexed. Then 10 ml of

doubly distilled water were added and the mixture was vortexed again. This mixture was allowed to stand overnight at -20°C until phase separation. The upper methanol-water phase and the lower chloroform phase were separated. The interface was saved for protein dosage. Both fractions were reduced under a nitrogen stream. The lipid extracts were reduced until total evaporation while the aqueous samples were lyophilized to dryness. Aqueous and lipid samples were stored at -20°C .

Before ^1H and ^{31}P NMR measurement of *aqueous* extracts, the dried aqueous residue was dissolved in 1 ml of D_2O and treated with the resin Chelex 100 (Sigma, St. Louis, MO). The mixture was vortexed and the resin was separated by centrifugation. Prior to ^{31}P NMR studies of the *lipid* extracts, samples were buffered (150 nM tricene buffer) and 6 mM EDTA (Fluka, Buchs, Switzerland) was added to minimize the interaction of the phosphate with the divalent ions. The dried chloroform residue was dissolved in a mixture of 0.8 ml of chloroform and 0.1 ml of methanolic EDTA and centrifuged.

MR spectroscopy

***In vivo* single-voxel ^1H magnetic resonance spectroscopy.** All imaging was performed on a 4.7 T horizontal bore MR imager (Bruker, Billerica, MA). Mice were positioned into a 24 mm i.d. Litzcage coil (Doty Scientific, SC). Volumes of interest (VOIs) were placed inside tumors according to T_2 -weighted reference images. VOIs ranged from 27 to 125 mm^3 depending on the tumor size and were placed to avoid signal contamination from surrounding tissue. Optimization of magnetic field homogeneity (localized shimming) was performed manually, achieving a linewidth of the water resonance below 15 Hz. Water suppression was achieved through a 15 ms Gaussian presaturation pulse centered at the water frequency³⁸ and proton MR spectra were obtained with a PRESS (point resolved spectroscopy³⁹) localization technique. Typical acquisition parameters were $TR = 4\text{ s}$, $TE = 136\text{ ms}$, data points = 4096, averages = 512, total acquisition time = 34 min 8 s. MR spectroscopic data were analyzed using XWIN-NMR software (Bruker). Signal intensities of choline-containing compounds (tCho, $\delta = 3.22\text{ ppm}$), creatine-containing compounds (tCr, $\delta = 3.01\text{ ppm}$) and 'lactate + lipids' peak (lac + lip, $\delta = 1.33\text{ ppm}$) were calculated by deconvolutions of the resonance lines in postprocessed Fourier spectra. Postprocessing included zero filling to 8K data points and time domain apodization with a Gaussian function (line-broadening = 20), Fourier transformation and phase and baseline corrections. Peak intensities were normalized with the intensity of the water peak of the non-water suppressed scan as described in other studies.⁴⁰

***In vivo* magnetic resonance spectroscopy of tumor extracts.** All spectra were recorded on a DRX-

500 high-resolution NMR spectrometer operating at 11.7 T (Bruker, Rheinstetten, Germany). The sample tube was spun at 16 Hz. Proton spectra were collected at 500.1 MHz and phosphorus spectra were recorded at 202.5 MHz. In addition to comparison with literature assignments, all signal assignments were made by adding pure substances of individual metabolites to sample solution and comparing peak heights before and after addition. The protein content of each tumor was determined using the Bradford assay.

^1H spectroscopy. A 0.4 ml volume of the aqueous extracts was transferred to 5 mm NMR tubes. The spectral parameters were: 90° pulse, 128 scans, 65K data points, sweep width = 10,330 Hz, temperature = 280°K , acquisition time = 3.17 sec, delay = 2 sec. A 5.7 mM solution of 3-(Trimethylsilyl)propionic acid (TSP) was used as an external standard for sample quantification. A line-broadening of 0.3 Hz was applied prior to Fourier transformation. Quantification was performed by comparing the integrated TSP signal with the signal of interest in the tumor spectrum after baseline and phase correction. The surface area of each peak was normalized to the number of contributing protons per molecule and to tumor protein content. Absolute concentrations are given as means \pm SEM in nmol/mg protein.

^{31}P spectroscopy. 0.4 ml of the lipid or of the aqueous extracts were transferred to 5 mm NMR tubes. For aqueous extracts, the acquisition parameters were: 90° pulse, 5000 scans, 65K data points, sweep width = 10,162 Hz, temperature = 280 K , acquisition time = 3.22 s, delay = 9 s. For non-aqueous extracts, the acquisition parameters were identical except that only 1200 scans were acquired. An 8.7 mM solution of 1-APP (1 aminopropylphosphonate) was used as an external standard. All free induction decays were subjected to 1 Hz apodization before Fourier transformation, phasing and baseline correction. Quantification was performed by comparing the integrated 1-APP signal with the signal of interest in the tumor spectrum. The surface area of each peak was normalized to the number of contributing phosphorus per molecule and to tumor protein content. Absolute concentrations are given as means \pm SEM in nmol/mg protein.

In vitro assays

Toxicity assay. Cells plated overnight in 96-well plates at a concentration of 1×10^6 per well were treated with a 5–500 μM range of PX-478 or media as control for 24 h under hypoxia. Plates were washed once in media then maintained for 48 h under regular incubation conditions. Cells were fixed with 0.025% glutaraldehyde (Sigma) for 30 min followed by 0.1% Crystal Violet (Sigma) stain for 60 min. Plates were washed twice with doubly distilled water and dried for 18 h with 1.0% acetic acid. Assay

plates were read by measuring the absorbance at 590 nm on a Microplate Reader (BioTek Instruments, Germany).

Glucose uptake assay. Cells were seeded in replicates of six in 24-well culture plates and grown to about 80% confluence in DMEM growth media (Invitrogen, Carlsbad, CA) supplemented with 10% fetal calf serum (Omega Scientific, Tarzana, CA). Cultures were treated with PX-478 and transferred to a 2% O₂ (hypoxic) culture incubator for 24 h. Plates were washed in glucose-free RPMI medium supplemented with 12 mM NaCHO₃ and 100 μM desferoxamine mesylate (DFO) iron chelating reagent (Sigma). Cells were then suspended in 4 μCi of [³H]-2-deoxy-D-glucose in RPMI medium supplemented with 5.56 mM D-(+)-glucose and 12 mM NaHCO₃ and incubated for 1 h in hypoxia. Disintegrations per minute (dpm) per nanomole were determined from samples of culture supernatant using a 5000TD series liquid scintillation counter (Beckman Coulter, Brea, CA). Cells were washed in glucose-free medium and lysed with 0.1 M NaOH for measurement of dpm per well from lysate sample. Remaining lysate was neutralized with 0.1 M HCl and assayed for protein concentration using Bradford Reagent (Pierce, Rockford, IL). Glucose consumption rates were expressed as nmol/min/mg protein.

Lactate production assay. Cells seeded in 96-well culture plates were grown to ~80% confluence in growth medium, washed in glucose-free RPMI, then treated with PX-478 diluted in RPMI medium supplemented with 5.56 mM D-(+)-glucose and 12 mM NaHCO₃. Cells were then transferred to hypoxia for 16 h. The presence of lactic acid was verified with lactate reagent (Sigma). Lactate production values were expressed as nanomoles of lactate from culture supernatant over time (minutes) and protein concentration (milligrams).

RESULTS

In vivo single-voxel ¹H magnetic resonance spectroscopy

An *in vivo* ¹H MR spectrum from a representative HT-29 tumor is shown in Fig. 1. The time courses of changes in the main metabolites observed *in vivo* are shown in Fig. 2. A significant reduction in the total choline (tCho) signal of the PX-478-treated group relative to pretreatment values was observed 12 and 24 h after treatment. *In vivo*, tCho may comprise signals from choline-containing compounds, such as glycerolphosphocholine (GPC), phosphocholine (PC) and choline itself, together with contributions from other metabolites, such as myoinositol, taurine and phosphoethanolamine. The total creatine (tCr) signal was not resolved in all spectra and was not quantified at all time points. Nonetheless, it could be measured at 0 and 24 h and no significant changes were

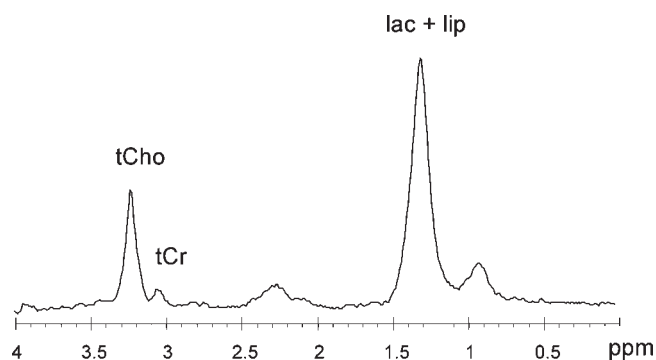


Figure 1. Typical *in vivo* single-voxel ¹H spectroscopy of HT-29 xenograft tumors. tCho, total choline; tCr, total creatine; lac + lip, lactate and lipid peak

observed (data not shown). Although the lactate and lipid (lac + lip) peak shows a trend to decrease, no significant change was observed at any time point, possibly owing to the variable contribution of the lipid content that results in a large variability of the measurement.

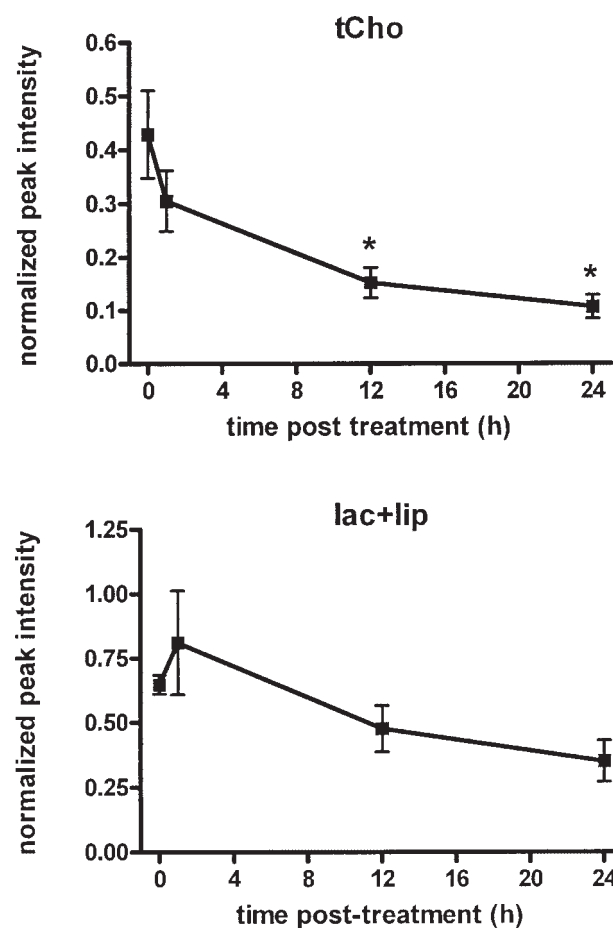


Figure 2. Relative quantification of (A) total choline (tCho) and (B) the lactate and lipid peak (lac + lip) with *in vivo* ¹H spectroscopy on HT-29 xenograft tumors before and up to 24 h following treatment with PX-478. Peak intensities were normalized with the intensity of the water peak of the non water suppressed scan. **p* < 0.05, Student's *t*-test. *N* = 10

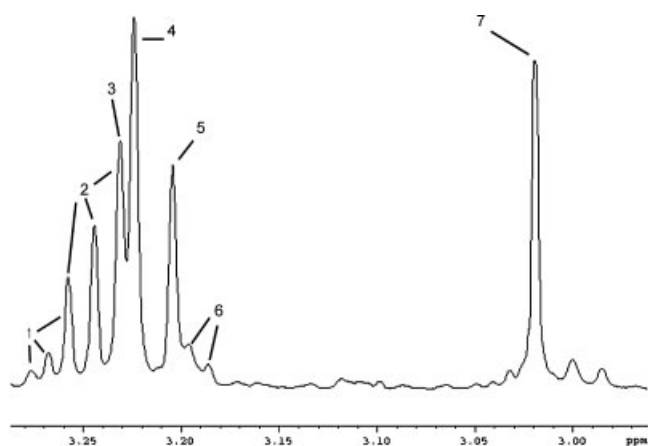


Figure 3. *Ex vivo* high-resolution ^1H spectrum of an HT-29 xenograft tumor aqueous extract (choline region, 3.34–2.94 ppm). 1, Myoinositol (myoI); 2, taurine (Tau); 3, glycerolphosphocholine (GPC); 4, phosphocholine (PC); 5, choline (Cho); 6, phosphoethanolamine (PE); 7, creatine (Cr)

***In vitro* magnetic resonance spectroscopy of tumor extracts**

In order to resolve the major components of the choline and lactate regions, we obtained *in vitro* high-resolution ^1H MR spectra of the aqueous extracts. The choline region of a typical *in vitro* ^1H MR spectrum (i.e. 3.34–2.94 ppm) is shown in Fig. 3. Concentrations of myoinositol (mI), taurine (Tau), choline (Cho), PC, GPC (with a contribution of Tau), creatine (Cr), alanine (Ala) and lactate (Lac) in tumor extracts were quantified. Of those metabolites, the levels of PC ($p = 0.02$), GPC ($p = 0.02$) and mI ($p = 0.05$) were significantly decreased in the PX-478-treated tumor extracts ($n = 8$) compared with vehicle-treated tumor extracts ($n = 3$) (Table 1), whereas changes in the other metabolites were insignificant. The

changes were observed at all doses (i.e. 50–150 mg/kg), where the higher doses were similar to the dose used for *in vivo* studies. Standard additions showed that Tau, mI and GPC were isochronous. For mI the upfield resonance was used for quantification and for Tau the middle peak was used. Extracts also allowed unequivocal assignment of the methyl lactate resonances. Consistent with the *in vivo* results, there was reduced lactate in the presence of drug, yet the differences did not reach significance (Table 1). This is in contrast to the effects of PX-478 on glucose uptake and lactate production *in vitro* (see below).

In vitro ^{31}P MRS of the aqueous extracts showed statistically significantly decreased levels of phosphoethanolamine (PE) ($p = 0.04$), PC ($p = 0.02$), glycerophosphoethanolamine (GPE) ($p = 0.01$) and GPC ($p = 0.03$) in the PX-478-treated tumors relative to the vehicle-treated tumors (Table 1). An expanded typical ^{31}P spectrum (i.e. 4.8–0.35 ppm) of the tumor aqueous extracts is presented in Fig. 4. Table 1 also shows that the changes observed for PC and GPC, two metabolites that are visible with both ^1H and ^{31}P MRS, are consistent with those two techniques and that the absolute amounts are in the same range. The fact that the values are slightly higher in the ^1H spectra might be due to the interference of other metabolites contributing to those peaks, such as Tau being partly underneath GPC and PC. However, the changes observed after treatment with PX-478 were similar with both ^1H and ^{31}P spectroscopy.

Finally, *in vitro* ^{31}P MRS of the lipid extracts allowed the quantification of most membrane phospholipids, such as phosphatidylethanolamine (PtdEtn), phosphatidylcholine (PtdCho) and its lyso derivative lyso-PtdCho, PtdCho plasmalogen, phosphatidylinositol (PtdI), sphingomyelin (SM) and cardiolipin (CL). An expanded typical ^{31}P spectrum (i.e. 0.3 to -1.0 ppm) of the tumor lipid extracts is presented in Fig. 5. SM and peak 4 were not always

Table 1. *In vivo* ^1H and ^{31}P MRS of HT-29 aqueous tumor extracts following vehicle or PX-478 treatment

Peak no.	Frequency (ppm)	Metabolites (nmol/mg tumor Pi)	Vehicle ($n = 3$)	PX-478 ($n = 8$)	p
<i>Fig. 3</i>					
^1H MRS					
1	3.271	mI	2.2 ± 0.5	1.1 ± 0.3	0.05
2	3.243	Tau	5.1 ± 1.2	3.4 ± 0.8	NS
3	3.234	GPC	17.9 ± 4.1	9.0 ± 1.5	0.02
4	3.228	PC	29.4 ± 6.0	12.8 ± 3.0	0.02
5	3.206	Cho	3.9 ± 1.5	3.8 ± 0.8	NS
7	3.023	Cr	36.2 ± 6.8	24.8 ± 3.6	NS
Not shown	1.477	Ala	11.9 ± 1.9	8.5 ± 1.1	NS
Not shown	1.333	lac	49.4 ± 8.9	38.9 ± 3.6	NS
<i>Fig. 4</i>					
^{31}P MRS					
1	4.360	PE	14.4 ± 3.1	8.7 ± 1.3	0.04
2	3.870	PC	23.5 ± 4.1	10.7 ± 2.2	0.02
4	1.045	GPE	7.6 ± 1.6	2.8 ± 0.6	0.001
5	0.490	GPC	13.7 ± 2.5	5.2 ± 1.1	0.003

Data are expressed as the mean ± SEM. mI, myoinositol; Tau, taurine; GPC, glycerophosphocholine; PC, phosphocholine; Cho, choline; Cr, creatine; Ala, alanine; lac, lactate; PE, phosphoethanolamine; GPE, glycerophosphoethanolamine; NS, not significant. Two-tailed unpaired *t*-test was used to compare changes between groups.

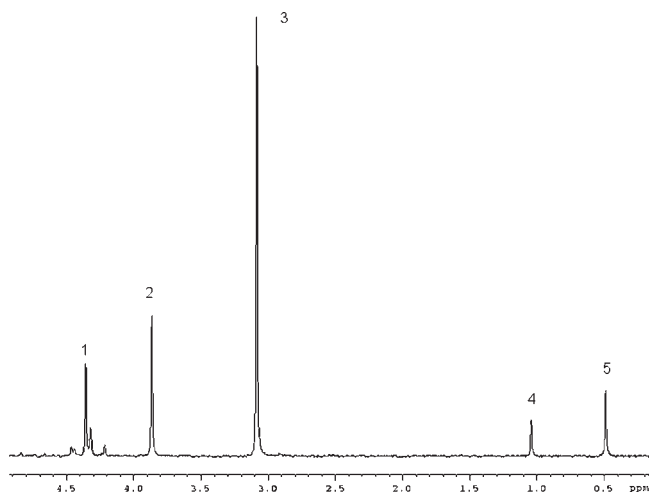


Figure 4. *Ex vivo* high-resolution ^{31}P spectrum of an HT-29 xenograft tumor aqueous extract (4.8–0.35 ppm). Peak 1, Phosphoethanolamine (PE); peak 2, phosphocholine (PC); peak 3, inorganic phosphate (Pi); peak 4, glycerophosphoethanolamine (GPE); peak 5, glycerophosphocholine (GPC)

resolved and were therefore not quantified. Among the other metabolites, significant decreases in CL, PtdEtn and PtdI were observed (Table 2). Two unidentified compounds were also significantly decreased.

In vitro cell metabolism

The *in vivo* and *ex vivo* ^1H MRS data showed an insignificant effect of PX-478 on lactate levels. This drug has been previously reported to inhibit the expression of the glucose transporter GLUT-1.²⁰ Therefore, we

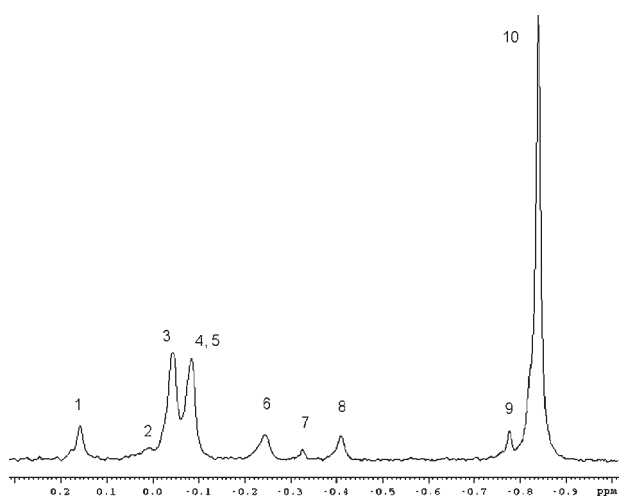


Figure 5. *Ex vivo* high-resolution ^{31}P spectrum of an HT-29 xenograft tumor lipid extract (0.3–1.0 ppm). Peak 1, cardiolipin (CL); peaks 2–4, unidentified; peak 5, sphingomyelin (SM); peak 6, phosphatidylethanolamine (PtdE); peak 7, lyso-PtdE; peak 8, phosphatidylinositol (PtdI); peak 9, phosphatidylcholine (PtdCho) plasmalogen; peak 10, PtdCho

further examined the effect of PX-478 on glucose metabolism *in vitro*. Treatment doses were similar to those reported previously. Briefly, PX-478 was non-toxic at concentrations up to $150\ \mu\text{M}$ for up to 16 h of exposure and $100\ \mu\text{M}$ for up to 48 h. Figure 6A shows that lactate production rates were significantly ($p < 0.05$) decreased by PX-478 at doses $> 20\ \mu\text{M}$ under hypoxic, but not normoxic, conditions. This is consistent with the action of this drug on HIF-1 α which is normally elevated under hypoxic conditions. Similarly, glucose consumption was significantly decreased at doses of 75 and $150\ \text{pmol/h/mg}$ in the presence of hypoxia [Fig. 6(B)].

DISCUSSION

We recently characterized the effect of PX-478 on dynamic contrast enhanced (DCE) and diffusion MRI *in vivo*.²¹ These data showed a dramatic reduction in tumor vascular permeability within 2 h and an increase in apparent diffusion within 24 h of PX-478 treatment. In this study, we further investigated *in vivo* and *ex vivo* MRS to characterize the metabolic response of tumors to this anti-HIF-1 α therapy.

Using *in vivo* ^1H spectroscopy, we were able to show a significant decrease in the tCho peak 12 and 24 after treatment with PX-478 and a lack of change in the tCr peak 24 h after treatment. *In vitro*, we were able to resolve most of the metabolites contributing to the 'choline region' with high-resolution spectroscopy and observed significant decreases in GPC, PC and myoI levels in the treated tumors. Elevated concentrations of choline metabolites are observed by MRS in a variety of malignancies and choline-derived metabolites undergo extensive alterations as a result of malignant transformation. (reviewed in Morse and Gillies⁴¹). For example, progression of tumor cells to a malignant phenotype has been associated with a reversal in the ratio of PC to GPC and an overall increase in the content of these two metabolites.³⁰ Enhanced choline transport and increased synthesis of PC were proven to be dominant pathways responsible for the elevated presence of choline metabolites in breast tumors.²² Glunde *et al.*²⁷ further identified increased choline kinase activity and also increased phospholipase C activity (catabolism) as the major factors responsible for elevated PC levels in breast cancers. Clinically, reduction in the tCho peak in response to neoadjuvant chemotherapy in breast cancer has been observed.⁴² tCho has also recently been tested as a predictive factor for clinical response of patients with locally advanced breast cancer.⁴³ Choline-kinase inhibitors are a potential chemotherapeutic target by blocking the production of phosphocholine.⁴⁴ Regarding myo-inositol, it has been reported to be elevated in breast-cancer tissue extracts in comparison with adjacent control tissue using the advanced data analysis technique of self-organizing maps.⁴⁵ It has also been shown to be elevated in high-grade

Table 2. *In vivo* ^{31}P MRS of HT-29 lipid tumor extracts following vehicle or PX-478 treatment

Peak no.	Frequency (ppm)	Metabolites (nmol/mg tumor Pi)	Vehicle (n = 3)	PX-478 (n = 8)	p
1	0.172	CL	4.1 ± 0.8	2.3 ± 0.9	0.04
2	0.151	2	2.0 ± 0.3	1.1 ± 0.1	0.01
3	-0.034	3	19.7 ± 2.1	11.3 ± 2.0	0.04
6	-0.201	PtdEtn	7.5 ± 2.0	2.6 ± 0.4	0.005
7	-0.323	lyso-PtdCho	1.3 ± 0.4	1.4 ± 0.6	NS
8	-0.389	PtdI	5.5 ± 1.9	1.8 ± 0.4	0.01
9	-0.777	PtdCho plasmalogen	2.9 ± 1.1	1.8 ± 0.2	NS
10	-0.84	PtdCho	51.5 ± 9.0	33.0 ± 6.5	NS

Data are expressed as the mean ± SEM. CL, cardiolipin; PtdEtn, phosphatidylethanolamine; PtdCho, phosphatidylcholine; PtdI, phosphatidylinositol; NS, not significant. Two-tailed unpaired *t*-test was used to compare changes between groups.

glioma³⁷ and in prostate cancer.⁴⁶ However, myo-inositol was also found decreased in some human colon carcinoma extracts.⁴⁷ Although consistent in some studies, the use of this metabolite as marker of non-brain tumor response is not yet accepted.

A peculiar ^{31}P spectral feature of aqueous tumor extracts is the prominent signals in the phosphomonoester (PME) and phosphodiester (PDE) frequencies, mainly constituted of PE and PC and of GPC and GPE, respectively.^{22,48} These have been studied as possible indicators of malignancy, tumor response to therapy and even predictors of long-term response.^{49–54} Our results show high basal levels of both PMEs and PDEs in aqueous extracts of HT-29 tumors that are significantly decreased after anti-tumor treatment with PX-478. This correlates well with Negendank *et al.*,⁵⁵ who described early decreases in PME signals as good predictors of response to either radio- or chemotherapy. Notably, Chung *et al.*⁵⁶ reported an increase in PC and PME levels

following treatment with the Hsp90 inhibitor 17AAG of HT-29 tumors that might indicate a particular mechanism of action for 17AAG which is not yet fully understood. PE has been shown to prevail over PC in breast, brain, liver cancers and lymphomas,⁵⁵ which is not the case in our study. PE/PC ratios of < 1.0 have been observed in cultured cells with high S-phase fractions.⁴⁸ We observe a ratio of 0.61 in the HT-29 tumor extracts that is not significantly modified after treatment (0.80). The PC/GPC ratio has been suggested as a possible indicator of altered PL turnover during tumor progression.^{30,57} This ratio was also not modified after treatment in our study. It is often assumed that increased pools of PCho and PE reflect intensified cell membrane synthesis, associated with accelerated tumor cell replication. However, the biochemical mechanisms underlying changes in the contents of PL metabolites are still not clear. Experiments to date suggest that not only biosynthetic pathways, but also mitogen- and oncogene-induced activation of PtdCho- and PtdEtn-specific phospholipases may contribute to the accumulation of PE and PC pools in tumor cells.^{27,48}

Regarding lipid extracts, significant decreases in CL, PtdEtn and PtdI were observed after treatment with PX-478. Merchant *et al.*⁵⁸ reported elevated levels of both PtdEtn and PtdI in malignant compared to benign samples of breast tissue. Sterin *et al.*⁵⁸ reported a lack of change in the phospholipid profile of MB231 cells cultured in matrigel after treatment with paclitaxel, yet a high concentration of adriamycin caused a decrease in PtdC in the same system. Increased malignancy in gliomas was shown to be accompanied by an increase of PtdC.⁶⁰

Finally, *in vitro* measurements showed a significant decrease in glucose consumption and also in lactate production under hypoxic conditions after treatment with PX-478. Although, until now, there have been no conclusive results regarding a relationship between lactate concentration and tumor malignancy, some groups have found that lactate concentrations have prognostic value in patients with gliomas or cervical cancers.^{61,62} A decrease in lactate in response to cyclophosphamide treatment was observed *in vitro* (on cells and tumor extracts) and also *in vivo* in RIF-1 tumors resulting

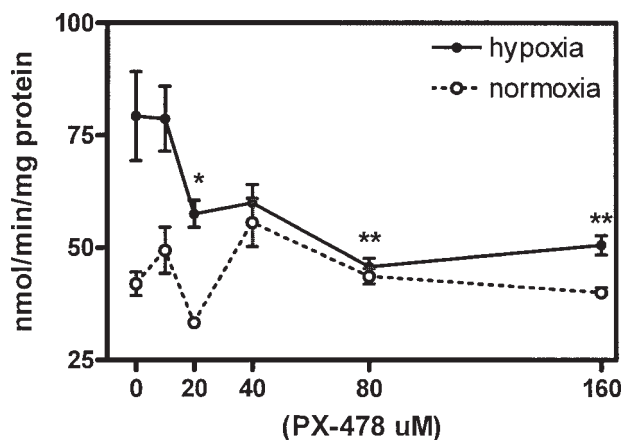


Figure 6. (A) *In vitro* lactate production rate in HT-29 cells with increasing doses of PX-478, under both normoxic and hypoxic conditions. **p* < 0.05, ***p* < 0.01, one-way ANOVA, Dunnett *post hoc* test, signification relative to the control data point (0 μM of PX-478). *N* = 8. (B) *In vitro* glucose consumption rate in HT-29 cells with increasing doses of PX-478 under hypoxic conditions. ***p* < 0.01, one-way ANOVA, Dunnett *post hoc* test, signification relative to the control data point (0 μM of PX-478). *N* = 6

from decreased glycolytic metabolism and an increase in tumor perfusion/permeability.⁶³

The lack of a significant effect of PX-478 on lactate levels in the current study is contrasted with the inhibition of glucose consumption and lactate production by this drug *in vitro*. It is possible that the effects of this drug are complicated *in vivo* by a direct inhibition of glycolysis, which would decrease lactate, coupled to decreased perfusion, which could lead to hypoxia and hence an increase in lactate production via reversal of the Pasteur Effect. Interestingly, Troy *et al.* have recently shown that extracts of HIF-1 α -deficient astrocytomas have slightly, yet significantly, lower lactate levels compared with wild type controls.⁶⁴ They observed lactate:water ratios of 2.06 vs 3.67 in lactate-edited *in vivo* spectra and 10.4 vs 11.9 $\mu\text{mol/g}$ wet wt in *ex vivo* extracts for the HIF-1 α knockouts and wild-type astrocytomas, respectively. These values are consistent with the current observations, suggesting that HIF-1 α inhibition depresses lactate levels. It remains a question in the current study whether the lack of statistical significance between the pre- and post-therapy lactate levels represent a true lack of an effect or type 1 or 2 statistical errors. Both *in vivo* and *ex vivo* data showed decreases in lactate resonances, yet failed to reach significance. The lack of a significant effect on *in vivo* spectra may have been caused by interference with the co-resonant lipid peak, which would be a type 1 (systematic) error. *Ex vivo*, variability in the processing of tumors for extracts may have contributed to the lack of significance, which would be a type 2 (non-systematic) error. This is being further examined *in vivo* using lactate editing during spectral acquisition. Nevertheless, the significant and robust change in tCho has identified this as a potential ¹H MRS-visible biomarker for drug response *in vivo* while high-resolution spectroscopy indicated that GPC, PC, myoI, PE, GPE, CL, PtdEtn and PtdI are potential *ex vivo* markers for drug response.

Acknowledgments

This work was supported by PHS grants U54 CA90821, CA077575 and infrastructure grants R24 CA083148 and P30 CAQ3074, CA98920. Kvar Black was supported by Beckman Scholars Program and the Undergraduate Biology Research Program. Ian Robey was supported by PHS training grant T32 HL 007249-29. Bénédicte Jordan was supported by the Belgian National Fund for Scientific Research (FNRS) as 'Chargé de Recherches'.

REFERENCES

- Hoeckel M, Schlenger K, Aral B, Mitza M, Schaffer U, Vaupel P. Association between tumour hypoxia and malignant progression in advanced cancer of the uterine cervix. *Cancer Res.* 1996; **56**: 4509–4515.
- Moulder J, Rockwell S. Tumor hypoxia: its impact on cancer therapy. *Cancer Metast. Rev.* 1987; **5**: 313–341.
- Goenewardene TI, Sowter HM, Harris AL. Hypoxia-induced pathways in breast cancer. *Micro. Res. Technol.* 2002; **59**: 41–48.
- Gatenby RA, Gillies RJ. Why do cancers have high aerobic glycolysis? *Nat. Rev.* 2004; **4**: 891–899.
- Chen J, Zhao S, Nakada K, Kuge Y, Tamaki N, Okada F, Wang J, Shindo M, Higashino F, Takeda K, Asaka M, Katoh H, Sugiyama T, Hosokawa M, Kobayashi M. Dominant-negative hypoxia-inducible factor-1 α reduces tumor-igenicity of pancreatic cancer cells through the suppression of glucose metabolism. *Am. J. Pathol.* 2003; **162**: 1283–1291.
- Hanahan D, Folkman J. Patterns and emerging mechanisms of the angiogenic switch during tumorigenesis. *Cell* 1996; **86**: 353–364.
- Semenza GL. Hypoxia, clonal selection and the role of HIF-1 in tumor progression. *Crit. Rev. Biochem. Mol. Biol.* 2000; **35**: 71–103.
- Powis G, Kirkpatrick L. HIF-1 α as a cancer drug target. *Mol. Cancer Ther.* 2004; **3**: 647–654.
- Chilov D, Camneish G, Kvietikova I, Ziegler U, Gassmann M, Wenger RH. Induction and nuclear translocation of hypoxia-inducible factor-1 α (HIF-1 α): heterodimerization with ARNT is not necessary for nuclear accumulation of HIF-1 α . *J. Cell Sci.* 1999; **112**: 1203–1212.
- Minchenko A, Salceda S, Bauer T. Hypoxia regulatory elements of the human vascular endothelial growth factor gene. *Cell. Mol. Biol. Res.* 1994; **40**: 35–39.
- Semenza GL. HIF-1: mediator of physiological and pathophysiological responses to hypoxia. *J. Am. Phys. Soc.* 2000; **88**: 1474–1480.
- Kallio PJ, Wilson WJ, O'Brien S, Makino Y, Poellinger L. Regulation of the hypoxia-inducible factor-1 α by the ubiquitin-proteasome pathway. *J. Biol. Chem.* 1999; **274**: 6519–6525.
- Zhong H, De Marco A, Laughner E, Lim M, Hilton D, Zagzag D, Buechler P, Isaacs WB, Semenza GL, Simons JW. Over-expression of hypoxia-inducible factor 1 alpha in common human cancers and metastases. *Cancer Res.* 1999; **59**: 5830–5835.
- Giatromanolaki A, Koukourakis M, Sivridis E, Turley H, Talks K. Relation of hypoxia inducible factor 1 alpha and 2 alpha in operable non-small cell lung cancer to angiogenicmolecular profile of tumors and survival. *Br. J. Cancer* 2001; **85**: 881–890.
- Birner P, Schindl M, Obermair A, Breitenecker G, Oberhuber G. Expression of hypoxia-inducible factor-1 alpha in epithelial ovarian tumors: its impact on prognosis and on response to chemotherapy. *Clin. Cancer Res.* 2001; **7**: 1661–1668.
- Bos R, van der Groep P, Greijer AE, Shvarts A, Meijer S, Pinedo HM, Semenza GL, van Diest PJ, van der Wall E. Levels of hypoxia-inducible factor-1 alpha independently predict prognosis in patients with lymph node negative breast carcinoma. *Cancer* 2003; **97**: 1573–1581.
- Aebersold DM, Burri P, Beer KT, Laissue J, Djonov V, Greiner RH, Semenza GL. Expression of hypoxia-inducible factor-1 alpha: a novel predictive and prognostic parameter in the radiotherapy of oropharyngeal cancer. *Cancer Res.* 2001; **61**: 2911–2916.
- Birner P, Schindl M, Obermair A, Plank C, Breitenecker G, Oberhuber G. Over-expression of hypoxia-inducible factor-1 alpha is a marker for an unfavorable prognosis in early-stage invasive cervical cancer. *Cancer Res.* 2000; **60**: 4693–4696.
- Zagzag D, Zhong H, Scalzetti J, Laughner E, Simons J, Semenza G. Expression of hypoxia-inducible factor-1 alpha in brain tumors: association with angiogenesis, invasion and progression. *Cancer* 2000; **88**: 2606–2618.
- Welsh S, Williams R, Kirkpatrick L, Paine-Murrieta G, Powis G. Antitumor activity and pharmacodynamic properties of PX-478, an inhibitor of hypoxia-inducible factor-1 alpha. *Mol. Cancer Ther.* 2004; **3**: 233–244.
- Jordan BF, Runquist M, Raghunand N, Baker A, Williams R, Kirkpatrick L, Powis G, Gillies RJ. 2005. Imaging the effects of hif-1 alpha inhibition by Diffusion and Dynamic Contrast Enhanced MRI. *Neoplasia* 2005; **7**: 475–485.
- Leach MO, Verrill M, Glaholm J, Smith TA, Collins DJ, Payne GS, Sharp JC, Ronen SM, McCready VR, Powles TJ, Smith IE. Measurements of human breast cancer using magnetic resonance spectroscopy: a review of clinical measurements and a report

- of localized ^{31}P measurements of response to treatment. *NMR Biomed.* 1998; **11**: 314–340.
23. Kurhanewicz J, Vigneron DB, Nelson SJ. Three-dimensional magnetic resonance spectroscopic imaging of brain and prostate cancer. *Neoplasia* 2000; **2**: 166–189.
 24. Ronen SM, Leach MO. Imaging biochemistry: applications to breast cancer. *Breast Cancer Res.* 2001; **3**: 36–40.
 25. Evelhoch JL, Gillies RJ, Karczmar GS, Koutcher JA, Maxwell RJ, Nalcioğlu O, Raghunand N, Ronen SM, Ross BD, Swartz HM. Applications of magnetic resonance in model systems: cancer therapeutics. *Neoplasia* 2000; **2**: 152–165.
 26. Nurenberg P, Sartoni-D'Ambrosia G, Szczepaniak LS. Magnetic resonance spectroscopy of renal and other retroperitoneal tumors. *Curr. Opin. Urol.* 2002; **12**: 375–380.
 27. Glunde K, Jie C, Bhujwalla ZM. Molecular causes of the aberrant choline phospholipid metabolism in breast cancer. *Cancer Res.* 2004; **64**: 4270–4276.
 28. Ackerstaff E, Pflug BR, Nelson JB, Bhujwalla ZM. Detection of increased choline compounds with proton nuclear magnetic resonance spectroscopy subsequent to malignant transformation of human prostatic epithelial cells. *Cancer Res.* 2001; **61**: 3599–3603.
 29. Katz-Brull R, Lavin PT, Lenkinski RE. Clinical utility of proton magnetic resonance spectroscopy in characterizing breast lesions. *J. Natl. Cancer Inst.* 2002; **94**: 1197–1203.
 30. Aboagye EO, Bhujwalla ZM. Malignant transformation alters membrane choline phospholipid metabolism of human mammary epithelial cells. *Cancer Res.* 1999; **59**: 80–84.
 31. Preul MC, Caramanos Z, Collins DL, Villemure JG, Leblanc R, Olivier A, Pokrupa R, Arnold DL. Accurate, noninvasive diagnosis of human brain tumors by using proton magnetic resonance spectroscopy. *Nat. Med.* 1996; **2**: 323–325.
 32. Cheng LL, Chang IW, Smith BL, Gonzalez RG. Evaluating human breast ductal carcinomas with high-resolution magic-angle spinning proton magnetic resonance spectroscopy. *J. Magn. Reson.* 1998; **135**: 194–202.
 33. Sitter B, Sonnewald U, Spraul M, Fjosne HE, Gribbestad IS. High-resolution magic angle spinning MRS of breast cancer tissue. *NMR Biomed.* 2002; **15**: 327–337.
 34. Katz-Brull R, Seger D, Rivenson-Segal D, Rushkin E, Degani H. Metabolic markers of breast cancer: enhanced choline metabolism and reduced choline-ether-phospholipid synthesis. *Cancer Res.* 2002; **62**: 1966–1970.
 35. Nelson SJ, Graves E, Pirzkall A, Li X, Antiniw Chan A, Vigneron DB, McKnight TR. *In vivo* molecular imaging for planning radiation therapy of gliomas: an application of ^1H MRSI. *J. Magn. Reson. Imaging.* 2002; **16**: 464–476.
 36. Howe FA, Opstad KS. ^1H MR spectroscopy of brain tumours and masses. *NMR Biomed.* 2003; **16**: 123–131.
 37. Fan G, Sun B, Wu Z, Guo Q, Guo Y. *In vivo* single-voxel proton MR spectroscopy in the differentiation of high-grade gliomas and solitary metastases. *Clin. Radiol.* 2004; **59**: 77–85.
 38. Haase A, Frahm J, Hanicke W, Matthaei D. ^1H NMR chemical shift selective (CHESS) imaging. *Phys. Med. Biol.* 1985; **30**: 341–344.
 39. Bottomley PA. Spatial localization in NMR spectroscopy *in vivo*. *Ann. N. Y. Acad. Sci.* 1987; **508**: 333–348.
 40. Bolan PJ, Meisamy S, Baker EH, Lin J, Emory T, Nelson M, Everson LI, Yee D, Garwood M. *In vivo* quantification of choline compounds in the breast with ^1H MR spectroscopy. *Magn. Reson. Med.* 2003; **50**: 1134–1143.
 41. Morse DL, Gillies RJ. Choline containing compounds as diagnostic, prognostic and therapeutic response indicators for breast cancer. In *Recent Advances in MR Imaging and Spectroscopy*, Jagannathan NR (ed.). Jaypee Brothers Medical Publishers: New Delhi, 2005; 345–397.
 42. Jagannathan NR, Kumar M, Seenu V, Coshic O, Dwivedi SN, Julka PK, Srivastava A, Rath GK. Evaluation of total choline from *in-vivo* volume localized proton MR spectroscopy and its response to neoadjuvant chemotherapy in locally advanced breast cancer. *Br. J. Cancer* 2001; **84**: 1016–1022.
 43. Meisamy S, Bolan PJ, Baker EH, Bliss RL, Gulbahce E, Everson LI, Nelson MT, Emory TH, Tuttle TM, Yee D, Garwood M. Neoadjuvant chemotherapy of locally advanced breast cancer: predicting response with *in vivo* (^1H) MR spectroscopy – a pilot study at 4 T. *Radiology* 2004; **233**: 424–431.
 44. Hernandez-Alcoceba R, Fernandez F, Lacal JC. *In vivo* antitumor activity of choline kinase inhibitors: a novel target for anticancer drug discovery. *Cancer Res.* 1999; **59**: 3112–3118.
 45. Beckonert O, Monnerjahn J, Bonk U, Leibfritz D. Visualizing metabolic changes in breast-cancer tissue using ^1H -NMR spectroscopy and self-organizing maps. *NMR Biomed.* 2003; **16**: 1–11.
 46. Garcia-Segura JM, Sanchez-Chapado M, Ibarburen C, Viano J, Angulo JC, Gonzalez J, Rodriguez-Vallejo JM. *In vivo* proton magnetic resonance spectroscopy of diseased prostate: spectroscopic features of malignant versus benign pathology. *Magn. Reson. Imaging.* 1999; **17**: 755–765.
 47. Moreno A, Arus C. Quantitative and qualitative characterization of ^1H NMR spectra of colon tumors, normal mucosa and their perchloric acid extracts: decreased levels of myo-inositol in tumours can be detected in intact biopsies. *NMR Biomed.* 1996; **9**: 33–45.
 48. Podo F. Tumour phospholipid metabolism. *NMR Biomed.* 1999; **12**: 413–439.
 49. Ghalohm J, Leach MO, Collins DJ, Mansi J, Sharp JC, Madden A, Smith IE, McCready VR. *In-vivo* ^{31}P magnetic resonance spectroscopy for monitoring treatment response in breast cancer. *Lancet.* 1989; **i**: 1326–1327.
 50. Tausch-Treml R, Baumgart F, Ziessow D, Kopf-Maier P. ^{31}P NMR spectroscopy of a xenografted hypopharynx carcinoma: effects of tumor growth and treatment with cisplatin on the tumor phosphorus metabolism, histology and cytokinetics. *NMR Biomed.* 1992; **5**: 127–136.
 51. de Certaines JD, Larsen VA, Podo F, Carpinelli G, Briot O, Henriksen O. *In vivo* ^{31}P MRS of experimental tumours. *NMR Biomed.* 1993; **6**: 345–365.
 52. Sijens PE, Eggermont AM, van Dijk PV, Oudkerk M. ^{31}P magnetic resonance spectroscopy as predictor of clinical response in human extremity sarcomas treated by single dose TNF-alpha + melphalan isolated limb perfusion. *NMR Biomed.* 1995; **8**: 215–224.
 53. Griffiths JR, Tate AR, Howe FA, Stubbs M. Magnetic resonance spectroscopy of cancer-practicalities of multi-centre trials and early results in non-Hodgkin's lymphoma. *Eur. J. Cancer.* 2002; **38**: 2085–2093.
 54. Arias-Mendoza F, Smith MR, Brown TR. Predicting treatment response in non-Hodgkin's lymphoma from the pretreatment tumor content of phosphoethanolamine plus phosphocholine. *Acad. Radiol.* 2004; **11**: 368–376.
 55. Negendank W. Studies of human tumors by MRS: a review. *NMR Biomed.* 1992; **5**: 303–324.
 56. Chung YL, Troy H, Banerji U, Jackson LE, Walton MI, Stubbs M, Griffiths JR, Judson IR, Leach MO, Workman P, Ronen SM. Magnetic resonance spectroscopic pharmacodynamic markers of the heat shock protein 90 inhibitor 17-allylamino-17-demethoxygeldanamycin (17AAG) in human colon cancer models. *J. Natl. Cancer Inst.* 2003; **95**: 1624–1633.
 57. Bell JD, Bhakoo KK. Metabolic changes underlying ^{31}P MR spectral alterations in human hepatic tumours. *NMR Biomed.* 1998; **11**: 354–359.
 58. Merchant TE, Kasimos JN, Vroom T, de Bree E, Iwata JL, de Graaf PW, Glonek T. Malignant breast tumor phospholipid profiles using (^{31}P) magnetic resonance. *Cancer Lett.* 2002; **176**: 159–167.
 59. Sterin M, Cohen JS, Mardor Y, Berman E, Ringel I. Levels of phospholipid metabolites in breast cancer cells treated with antimetabolic drugs: a ^{31}P -magnetic resonance spectroscopy study. *Cancer Res.* 2001; **61**: 7536–7543.
 60. Lehnhardt FG, Rohn G, Ernestus RI, Grune M, Hoehn M. ^1H - and (^{31}P)-MR spectroscopy of primary and recurrent human brain tumors *in vitro*: malignancy-characteristic profiles of water soluble and lipophilic spectral components. *NMR Biomed.* 2001; **14**: 307–317.
 61. Tarnawski R, Sokol M, Pieniazek P, Maciejewski B, Walecki J, Miszczyk L, Krupska T. ^1H -MRS *in vivo* predicts the early treatment outcome of postoperative radiotherapy for malignant gliomas. *Int. J. Radiat. Oncol. Biol. Phys.* 2002; **52**: 1271–1276.

62. Walenta S, Wetterling M, Lehrke M, Schwickert G, Sundfor K, Rofstad EK, Mueller-Klieser W. High lactate levels predict likelihood of metastases, tumor recurrence and restricted patient survival in human cervical cancers. *Cancer Res.* 2000; **60**: 916–921.
63. Poptani H, Bansal N, Graham RA, Mancuso A, Nelson DS, Glickson JD. Detecting early response to cyclophosphamide treatment of RIF-1 tumors using selective multiple quantum spectroscopy (SelMQC) and dynamic contrast enhanced imaging. *NMR Biomed.* 2003; **16**: 102–111.
64. Troy H, Chung Y-L, Madhu B, Mayr M, Ly L, Blouw B, Johnson R, Griffiths JR, Stubbs M. A metabolomic study of wild type and HIF-1 α deficient astrocytomas measured by *in vivo* and *in vitro* 1H MRS. *Proc. ISMRM* 2005; **13**: 2040.